MedCrave
Step into the World of Research
International Journal of Petrochemical Science & Engineering

Research Article

Open Access

CrossMark

Application of corrosion-resistant Corning advanced-flow reactors for multiphase Bunsen reaction - Part one: Investigation on SO_2 absorption

Abstract

Bunsen reaction ($2H_2O + I_2 + SO_2 \rightarrow H_2SO_4 + 2HI$) is a center reaction of two important chemical cycles for hydrogen production: the H_2S splitting cycle and the sulfur-iodine (S-I) water-splitting cycles. Introducing I_2-tolune solution to the reaction can ease challenges such as side reactions and corrosion hazard. The glass-made Corning® Advanced-Flow™ Reactor (AFR) can completely avoid corrosion and also improve the mass transfer among the multiphase, i.e., gas SO_2-N_2, water, and toluene-I_2, to produce HI/H_2SO_4. In this paper, the absorption behavior of SO_2 in water, toluene and water-toluene mixture was investigated in the absence of iodine. The influences of mole fraction of SO_2 in gas phase and the flow rates of gas and liquid on SO_2 absorption rate and liquid-side volumetric mass transfer coefficients showed different absorption behaviors of SO_2 molecules in water and toluene. The differences also appeared between the microscale and milliscale AFRs. However, the plot of the liquid-side volumetric mass transfer coefficient vs. residence time indicated straightforward and seamless scalability of the AFR from microscale to milliscale for SO_2-water and SO_2-toluene absorption. This absorption study was necessary to provide preliminary data for the multiphase Bunsen reaction investigation in which iodine is present.

Keywords: bunsen reaction, H_2S splitting cycle, hydrogen production, Corning glass advanced-flow™ reactor, liquid-side volumetric mass transfer coefficient

Volume 4 Issue 4 - 2019

Armin Moniri,[1#] Hui Wang,[1] Xinjun (Eric) Wu[2]

[1]Department of Chemical and Biological Engineering, University of Saskatchewan, Saskatoon, SK, Canada S7N 5A9

[2]Corning Reactor Technology Center (China), Changzhou, Jiangsu, China

Correspondence: Hui Wang, Department of Chemical and Biological Engineering, University of Saskatchewan, Saskatoon, SK, Canada S7N 5A9, Email hui.wang@usask.ca

#Current Address: Department of Natural Resources Canada, CanmetENERGY, Devon, AB, Canada T9G, 1A8, Canada

Received: July 19, 2019 | **Published:** July 31, 2019

Introduction

To upgrade bitumen from Canadian oil sands into synthetic crude oil, a tremendous amount of hydrogen (H_2) is needed mostly for hydrotreating, where nearly the same amount of hydrogen sulfide (H_2S) is produced on molar basis. Traditionally, the H_2S is converted into elemental sulfur (S) in sulfur recovery units through the Claus process.[1] Although the Claus process is very well established, it has drawbacks. For instance, about half of the H_2S handling costs are related to the tail gas treatment. More importantly, the conversion of hydrogen into low-value water reduces plant efficiency. An H_2S chemical splitting cycle[2] was developed in our research group in order to directly decompose hydrogen sulfide with simultaneous production of hydrogen, which could be reused in oil sands upgrading as a partial substitute for steam reforming of methane (SRM). Similar to the S-I water-splitting cycle,[3] this cycle consists of three chemical reactions:

$$H_2S + H_2SO_4 \rightarrow S + SO_2 + 2H_2O \left(120\text{–}150^oC\right) \quad (1)$$

$$2H_2O + I_2 + SO_2 \rightarrow H_2SO_4 + 2HI \left(25^oC\right) \quad (2)$$

$$2HI \rightarrow H_2 + I_2 \left(25^oC\right) \quad (3)$$

The overall reaction is:

$$H_2S \rightarrow H_2 + S \quad (4)$$

By further oxidizing the elemental sulfur produced from reaction (1) into SO_2, the cycle can produce two moles of H_2 from one mole of H_2S, leading to the production of one mole of sulfuric acid.[2] Reaction (2), known as the Bunsen reaction, and reaction (3), known as HI decomposition, are two of the three reactions in the S-I water-splitting cycle. These reactions have been widely studied since the S-I cycle was proposed, in particular, the Bunsen reaction, which links the sulfur and iodine loops in the S-I water-splitting cycle, has received remarkable attention recently through massive investments in research.[4–6] Initially, General Atomics (GA) proposed the following stoichiometry:

$$SO_2 + 16H_2O + 9I_2 \rightarrow \left(2HI + 10H_2O + 8I_2\right)_{HIx\ phase} + \left(H_2SO_4 + 4H_2O\right)_{sulfuric\ acid\ phase} \quad (5)$$

where, a large amount of iodine and water is required to prevent side reactions[3] and to separate the two acid products into two immiscible liquid phases: sulfuric acid (upper phase), mainly a mixture of H_2SO_4 and water, and hydroiodic acid (lower phase), including HI, I_2, and water.[7] Excessive use of water and iodine, according to the stoichiometry of reaction (5), results in increased capital and operating costs because of the excessive material circulation and reduced energy efficiency of the entire chemical cycle. For instance, high heat duty is required for the concentration of both acids prior to decomposition.[6] In addition, the Bunsen reaction must be carried out

at elevated temperatures above the melting point of iodine (117°C), leading to iodine vapor deposition in the setup and tube blockage. At the elevated temperatures, the severe corrosive of the Bunsen reaction products is also a major concern.[8] Therefore, experimental and theoretical research activities have been carried out during the last decade to minimize Bunsen reaction challenges.[9–12] Our research group recently proposed a low-temperature process for the H_2S splitting cycle where toluene is used to simply dissolve iodine and this dissolved iodine can be transported from I_2-toluene solution to aqueous phase such that the Bunsen reaction can be carried out continuously at room temperature.[13]

This low-temperature process avoids the side reactions and iodine vapor deposition, and prevents corrosion. Subsequent electrolysis of the Bunsen reaction products relieves concerns about product acids separations as well. Despite all the benefits, the use of an I_2-toluene solution leads to a multiphase reaction system involving gas, aqueous, and organic solutions, denoted as a gas-liquid-liquid system. In the multiphase reaction system, mass transfer across phases may become rate-limiting. The overall rate is proportional to the liquid-side volumetric or overall mass transfer coefficient (K_La). Usually, generation of high shear in the liquid near the interface and large interfacial areas are desirable in order to achieve high mass transfer rates.[14] Therefore, the apparent reaction rate of the Bunsen reaction was studied in the gas-liquid-liquid multiphase system using a batch reactor.[15] Comparisons of the rate of SO_2 absorption in the liquids of different compositions (toluene, toluene and water, I_2-toluene solution, water), indicated that SO_2 dissolution in liquid phase was the rate-controlling step provided the gas phase resistance was negligible. This was confirmed by the small value of the activation energy (6.02 kJ mol^{-1}) obtained by fitting the reaction rate at various temperatures using the Arrhenius equation. It was concluded that improvement of cross-phase mass transfer is critical to increase process efficiency.

The emerging new reactor technology, Corning® Advanced-Flow™ Reactor, was claimed to be capable of improving the gas-liquid mass transfer coefficients compared to other gas-liquid contactors such as bubble columns and spray columns.[16] The AFRs are made of glass or ceramic materials that are highly corrosion-resistant for aqueous acid solutions. The modular design of these AFRs allows scale-up from the lowest flow rate (10 mL min^{-1}) of the low-flow (LF) cells to highest flow rate (5000 mL min^{-1}) of the G4 cells. In addition, AFRs can improve heat transfer effectively.[17–19] To investigate the gas-liquid-liquid multiphase system of the Bunsen reaction where I_2 was provided for the Bunsen reaction through I_2-toluene solution, two types of AFRs, AFR-LF (maximum through-put: 5 m^3/year) and AFR-G1 (maximum through-put: 80 m^3/year), were chosen. The work is reported under one general title, divided into part one and part two. Part one, the present paper, deals with the absorption of SO_2 in water, toluene and water-toluene mixture to study the behaviors of multiphase system in the absence of iodine (Bunsen reaction). By applying two-film theory, the liquid-side volumetric mass transfer coefficients were calculated for the binary systems. The results for the two scales of AFRs (LF and G1) were also compared. With iodine added to SO_2-water-toluene mixture, part two studied the effects of operating conditions such as gas and liquid flow rates, water-to-toluene ratio, and temperature on SO_2 absorption and of I_2 consumption in continuous mode in both LF and G1.

Experimental

The experiment with the AFR-LF was conducted and analyzed at the University of Saskatchewan (UofS). The experiment using the AFR-G1, a larger commercially available module, was performed at the Corning Reactor Technology Center (CRTC) in Changzhou, China, while the analyses were performed in the Department of Biochemical Engineering, Changzhou University, Changzhou, China.

I. Experimental setups and operating conditions

The flow pathway of the AFRs consists of identical small heart-shaped cells in blue color as shown in Figure 1. Each module has variable cross sections, which cause the fluid to form a jet and repeat splitting and mixing actions along the pathway (divergent-convergent configuration).[16] This mechanism helps to increase the contact area among the phases. Commercial AFRs are designed in different sizes (LF, G1, G2, G3, and G4) depending on the state of the research and/or the scale of production throughput. The interconnected fluidic module design allows the use of several modules in cascades for multiple-step reactions. Each glass module is sandwiched between two fluid-heating plates, thus enabling temperature control.[20] Figure 1 also shows the experimental set up with AFR-LF modules and their connections used in this study.

The internal volume of each fluidic module of the AFR-LF is about 0.4mL, which allows for liquid flow rates in the range of 0–10mL min^{-1}. Fluidic modules may be used in parallel or series, depending on the research requirements. At the beginning, five modules were used in series: Module 1 had two fluid inlet ports (A_1 and A_2), allowing two fluids to mix and/or react. Module 2 had one inlet port (A_3), allowing a third fluid to be introduced and conditioned to the same temperature. For experiments at room temperature, this module seemed useless. Modules 4 and 5 (when necessary) were used to extend the residence time. In later runs, one module was used for SO_2 absorption to reduce residence time. For a typical run, a gas mixture of SO_2 and N_2, supplied from cylinders and controlled by two mass flow controllers (1179A Mass-Flo®, MKS), was fed to port A_2. Water and toluene were also pumped into the AFR-LF via ports A_1 and A_3 or A_3 and A_1, using 100-Legato KD scientific syringe pumps.

The experiments with AFR-LF were carried out at room temperature (22–25°C), at different gas flow rates ranging from 53.6 to 85.7 mL min^{-1} at standard temperature and pressure (STP) and at different liquid flow rates (water from 0.3 to 0.7 mL min^{-1} and toluene from 0.65 to 1.3mL min^{-1}). The outlet of the AFR-LF was open to the atmosphere. A manual control valve was designed to keep the level of the liquid constant at the lower-middle of the separator so that the outlet gas can be easily purged only from the top of the separator to an online GC for analysis. At the bottom of the separator, liquid was collected in a separatory funnel where the organic phase was sampled using a glass Pasteur pipet and the water phase was sampled from the bottom. The experiment setup with AFR-G1 was similar to what Figure 1 shows, except that the gas samples were collected by using Cole-Parmer Tedlar bags at specific time intervals and analyzed by using an off-line instrument. The internal volume of each fluidic module of the AFR-G1 is about 20 times that of the AFR-LF, i.e., 8 mL, with a maximum allowable liquid flow rate of 200mL min^{-1}. The rest of the conditions, such as material, geometry, and design conditions, remained unchanged.

Citation: Moniri A, Wang H, Wu X. Application of corrosion-resistant corning advanced-flow reactors for multiphase Bunsen reaction-part one: investigation on SO_2 absorption. *Int J Petrochem Sci Eng.* 2019;4(4):123–136. DOI: 10.15406/ipcse.2019.04.00112

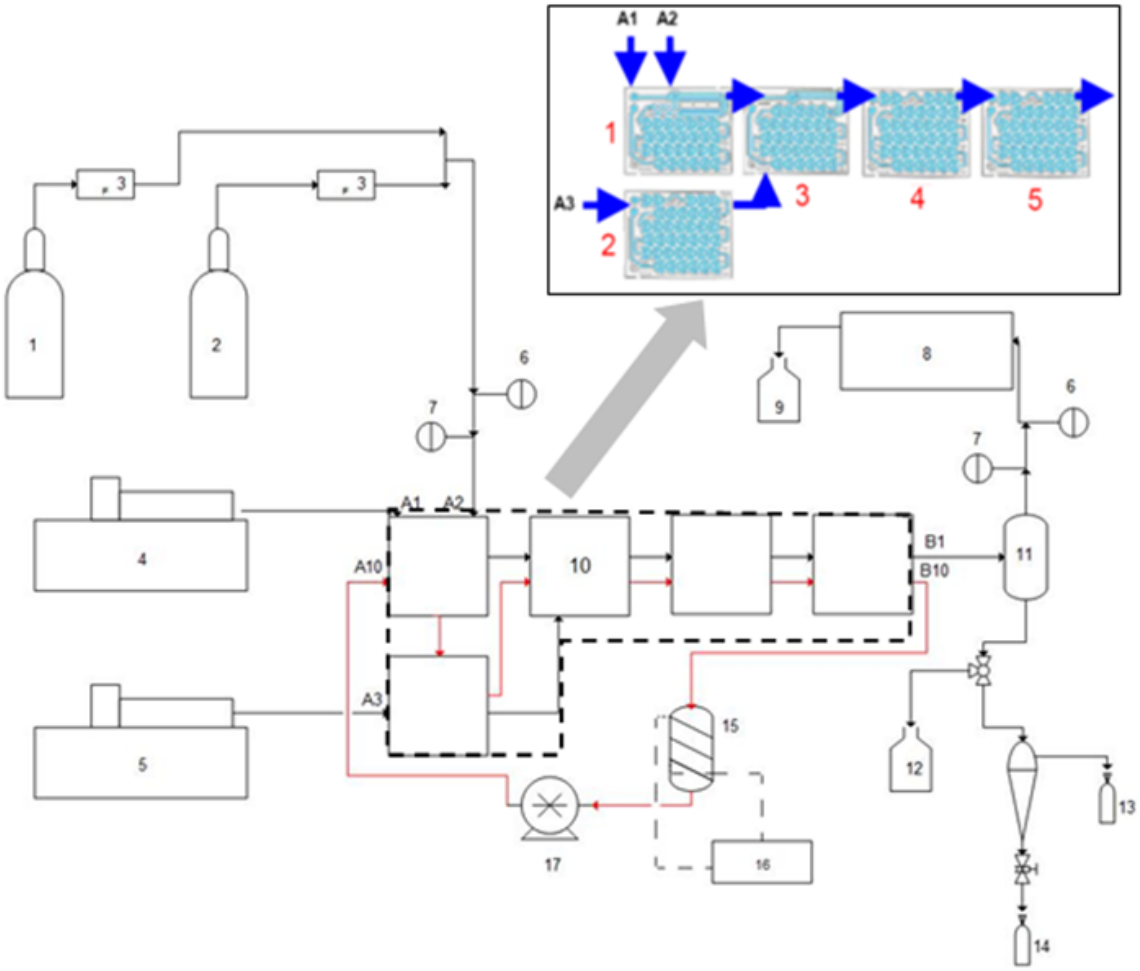

Figure 1 Schematic diagram of experimental setup for the Bunsen reaction using AFR-LF: (1) N_2 tank; (2) SO_2 tank; (3) Mass flow controller; (4) Organic syringe pump; (5) Water syringe pump; (6) Pressure indicator; (7) Temperature indicator; (8) Gas Chromatograph; (9) Scrubber; (10) Corning AFR-LF; (11) Gas-liquid separator; (12) Waste tank; (13) Organic phase sampling vial;(14) Water phase sampling vial; (15) water (oil) bath; (16) Temperature controller; and (17) Hot fluid pump.

For this study two fluidic modules (modules 1 and 3) were usually used. Module 1 was used for mixing of two feeds, usually SO_2-N_2 and the organic phase, and module 3 was used for introducing water and mixing. As in the runs by using the AFR-LF, the gas mixture of SO_2 and N_2, from cylinders controlled by two mass flow controllers (5850S Smart Mass low, Brooks Instruments Inc.). Toluene and water were also pumped into the AFR-G1 by using a PTFE pump (Fuji Technic Tokyo) and a stainless steel pump (Jiangsu Hanbon Science & Technology Co.), respectively. The experiments were carried out at room temperature (22–25°C), at different gas flow rates ranging from 1600 to 2000 mL min^{-1} at standard temperature and pressure (STP), and at different liquid flow rates (water from 30 to 60 mL min^{-1} and toluene from 37 to 79 mL min^{-1}). The outlet of the AFR-G1 was also open to atmospheric pressure. Two 10L bottles of concentrated sodium hydroxide (5 mol L^{-1}) were used in series to capture non-reacted SO_2 at the outlet of AFR-G1.

II. Chemicals

Chemicals used for the experiments with the AFR-LF were mostly ACS grade as received: sulfur dioxide (99.98%, Praxair), nitrogen (99.99%, Praxair), sodium hydroxide (97%, EMD), toluene (99.95%, BDH), and phenolphthalein and thyodene as the indicators. Chemicals were used as received without any modification or further steps of purification for the experiments with the AFR-G1 as well: sulfur dioxide (99.99%, Shanghai Weichuang Gas), nitrogen (99.999%, Changzhou Wujin Huayang Gas), sodium hydroxide (96%, Sinopharm Chemical Reagent), toluene (99.5%, Sinopharm Chemical Reagent), and phenolphthalein and thyodene were used as indicators. All the solutions used in both series of experiments and analyses were prepared by diluting the corresponding chemicals with deionized water.

III. Measurement techniques and analysis methods

For the experiments conducted using the AFR-LF, unreacted SO_2 was analyzed using a Varian CP-3800 gas chromatograph equipped with a thermal conductivity detector (TCD) after reaching steady state, roughly when the equivalent of three times the internal volume of the AFR-LF (or AFR-G1 in later experiments) had been processed. The internal normalization method was used for the gas calibration because this technique corrects for the sample-size error.[21] However, for the experiments conducted using the AFR-G1, the external calibration method was used. Due to unavailability of the online method, gaseous sulfur dioxide samples were collected in Cole-Parmer Tedlar bags and were then analyzed using a Taizhou Zhonghuan Analysis Instrument

Citation: Moniri A, Wang H, Wu X. Application of corrosion-resistant corning advanced-flow reactors for multiphase Bunsen reaction-part one: investigation on SO_2 absorption. *Int J Petrochem Sci Eng.* 2019;4(4):123–136. DOI: 10.15406/ipcse.2019.04.00112

Co. RPP-2000S Fluorescence Sulfur instrument at Changzhou University. Because the N_2 flow rate remains unchanged during absorption or reaction, the SO_2 flow rate in gas after absorption can be determined once its concentration in gas stream is known. The SO_2 absorption rate with respect to SO_2 can then be determined from the difference between the inlet and outlet SO_2 flow rates.

Results and discussion

I. Liquid-side volumetric mass transfer coefficient by applying two-film theory in AFRs

The two-film theory of mass transfer was used to determine the mass transfer coefficients of SO_2 across the gas/water and gas/toluene interfaces. According to this theory,[22] the flux of the mass transfer of gas molecules A (SO_2 in this case) into liquid through the interface (z=0) can be written as:

$$N_{A,z=0}=\frac{P_A-H_A C_A}{\frac{1}{k_G}-\frac{H_A}{k_L}}=K_G\left(P_A-P'_A\right) \text{ or } =\frac{\frac{P_A}{H_A}-C_A}{\frac{1}{k_G H_A}-\frac{1}{k_L}}=K_L\left(C'_A-C_A\right) \quad (6)$$

where N_A is the molar flux of A molecules from gas to liquid in the direction perpendicular to the mass transfer interface (mol·m^{-2}s^{-1}), P_A is the partial pressure of A in gas phase (Pa), H_A is Henry's law constant (Pa m^{3}mol^{-1}), C_A is the concentration of A in liquid (mol m^{-3}), k_G is the mass transfer coefficient in the gas phase (mol m^{-2}s^{-1}Pa^{-1}) and k_L is the mass transfer coefficient in the liquid phase (m s^{-1}); $P'_A = H_A C_A$, and $C'_A = P_A/H_A$, K_G (mol Pa^{-1}m^{-2}s^{-1}) is the liquid-side volumetric mass transfer coefficient based on partial pressure driving force and K_L (ms^{-1}) is the liquid-side volumetric mass transfer coefficient based on liquid driving force. As explained later, the ideal plug-flow is assumed for liquid and gas through the fluid channels of both the LF and G1, and the performance equation is developed by combing the rate equation with the material (mole) balance. Taking a slice of the reactor along the material flow direction as the volume element (dV) for mass balance, of which the interface area per volume is a (m^{2}m^{-3}, or m^{-1}),

$$\text{A lost in gas phase} = -F_G dy_A = \text{A gained in liquid} = \frac{F_L}{C_t} dC_A = N_{A,z=0} a dV \quad (7)$$

where, F_G and F_L are the total molar flow rates of gas and liquid (mol·s^{-1}), respectively, and C_t is the total concentration of liquid (mol m^{-3}). Considering $y_A = P_A/P_t$ (P_t is the total pressure of gas), and combining Eqs (6) and (7), integration on either side gives the reactor volume (V_r).

$$V_r = \frac{F_G}{K_G a.P_t}\int_{P_{A1}}^{P_{A2}} \frac{dP_A}{\left(P_A-P'_A\right)} = \frac{F_L}{K_L a.C_t}\int_{C_{A1}}^{C_{A2}} \frac{dC_A}{\left(C'_A-C_A\right)} \quad (8)$$

Upon integration of the liquid-side equation from inlet (C_{A1}) to outlet (C_{A2}), the liquid-side volumetric mass transfer coefficient ($K_L a$) becomes

$$K_L a = \frac{1}{\tau}\ln\frac{C^*_A-C_{A1}}{C^*_A-C_{A2}} = \frac{1}{\tau}\ln X \quad (9)$$

where, C^*_A is the equilibrium concentration of SO_2 in liquid phases (water or toluene) corresponding to the partial pressure of SO_2 in the gas phase at the inlet ($P_{SO2\ in}$), C_{A1} is the concentration of SO_2 in the liquid phase at the inlet, which is always zero, τ is the residence time of the liquid flow in the AFR ($V_r C_t/F_L$), and $K_L a$ is the liquid-side volumetric mass transfer coefficient. C^*_{A1} is calculated based on the partial pressure of SO_2 at the AFR inlet using Henry's law; C^*_{A2} is obtained at the AFR outlets based on the dissolved SO_2 (the difference between SO_2 inlet and outlet in the gas phase and the liquid flow). Considering the residence time of the liquid, the liquid-side volumetric mass transfer coefficients in the LF and G1 at different operating conditions are estimated by Eq. (9). In fact, Eq. (9) has been used to calculate $K_L a$ in microscale and milliscale AFR, not only for gas-liquid adsorption systems but also for liquid-liquid absorption systems.[23] The volumetric mass transfer coefficient ($K_L a$) is given because the liquid-side volumetric mass transfer coefficient based on liquid driving force, K_L, and the specific interface area, a, cannot be separated from each other and the determination of a is not within the scope of this study.

II. Flow regime analysis

The specific design of AFRs is somewhat different from what is normally observed for straight channels. When the fluid enters the heart-shaped cells it hits the first curved post and splits into two streams until reaching a second cylindrical post where the two streams recombine.[16] Therefore, for hydrodynamics study, the neck of the heart cell (H=400µm, W=300µm for the AFR-LF and H=1.12mm, W=1mm for the AFR-G1) is considered as the reference to define dimensionless parameters such as the Reynolds number.

$$Re = \frac{\rho u D_h}{\mu} \quad (10)$$

where ρ and µ are the average density and viscosity of the fluids, respectively, u is the total superficial velocity of the two phases, and D_h is the hydraulic diameter. The diameter of the fluid channel at the connection of the two heart-shaped cells in an AFR is used for D_h. The density and viscosity of the fluids used are given in the densities of water, toluene and sulfur dioxide gas at 20°C are 998.2, 886.89, and 2.71kg m^{-3}, respectively; the viscosities of them are 1.0×10^{-3}, 0.59×10^{-3}, and 1.25×10^{-5} Pa s, respectively.

Thus, for the AFR-LF, the gas and liquid flow rates range from 50 to 80 and 0.3 to 0.7 ml min^{-1}, respectively, and the range of the two-phase Re is from 2360 to 3790, which is just above the critical value implying the transition to turbulent flow. For the AFR-G1, Re ranges from 12820 to 16320 for SO_2 and water flow rates within 800-1000 and 30-60 mL , respectively, indicating fully developed turbulent flow. The visualization experiments, which were done for a CO_2-water system by Nieves-Remacha et al.,[16] using a AFR-G1, observed that two-phase flow in the AFR included a sequence of dynamic events: detachment, elongation, deformation, breakup, and coalescence of bubbles as they passed through the continuous phase. Confined geometry, small dimensions, and the presence of obstacles that disturb were mainly responsible for these events. Although these dynamic events were quite different from what had been observed in either stirred vessels or straight micro channels, tracer experiments for families of the AFR-LF and AFR-G1 showed the residence time distribution (RTD) to be narrow.[24] This indicates that each heart-shaped cell can be considered as an ideal stirred vessel in which complete mixing occurs. However, there must be no back mixing among cells and therefore, the flow throughout the whole AFRs can be treated as plug flow.

Citation: Moniri A, Wang H, Wu X. Application of corrosion-resistant corning advanced-flow reactors for multiphase Bunsen reaction-part one: investigation on SO_2 absorption. *Int J Petrochem Sci Eng.* 2019;4(4):123–136. DOI: 10.15406/ipcse.2019.04.00112

Table 1 SO_2 absorption rate measured in AFR-LF at different inlet positions of gas and liquids (water flow rate=0.5mL min^{-1}, toluene flow rate=0.5mL min^{-1}, gas flow rate=85mL min^{-1}, SO_2 mole fraction=0.824, T=22-25°C).

A_1	A_2	A_3	SO_2 outlet flow rate (mL min^{-1})	SO_2 outlet mole fraction	SO_2 absorption rate (mol $m^{-3}s^{-1}$)
water	SO_2-N_2	toluene	16.5	0.5239	15.02
toluene	SO_2-N_2	water	16.55	0.5246	15
toluene	water	SO_2-N_2	16.43	0.5228	15.04

Table 2 SO_2 absorption rate measured in AFR-LF at different inlet positions of gas and liquids (water flow rate = 0.1mL min^{-1}, toluene flow rate=0.9mL min^{-1}, gas flow rate=85mL min^{-1}, SO_2 mole fraction=0.824, T=22-25°C).

A_1	A_2	A_3	SO_2 outlet flow rate (mL min^{-1})	SO_2 outlet mole fraction	SO_2 absorption rate (mol $m^{-3}s^{-1}$)
SO_2-N_2	toluene	water	13.56	0.4749	15.84
SO_2-N_2	water	toluene	13.35	0.471	15.9
toluene	water	SO_2-N_2	13.39	0.4717	15.89

III. The effect of changing feeding position of reactants

The AFR-LF was chosen to test the effect of mixing order of the gas mixture of N_2 and SO_2, water, and toluene, using the port combinations of A_1, A_2, and A_3, which allow mixing of any two fluids in the first module and mixing of the third in the second module. Along with the six possible combinations of mixing as well as the other experimental variables, the absorption rate results are given in Tables 2 and 3. Absorption runs at a gas flow rate of 85mL min^{-1} at STP, SO_2 mole fractions (y_{SO2}=0.824), and two levels of water and toluene flow rates were conducted at room temperature. The results indicate that the SO_2 absorption rate by the liquid was independent of the feeding positions of the fluids. However, the slightly higher absorption rate in the latter Table was due to the higher toluene-to-water ratio. More toluene, which has the higher SO_2 solubility, would lead to a higher absorption rate. Although the same absorption rate can be achieved by either feeding sequence in the SO_2-water-toluene system, to maintain consistency in the experiments, the first and second feeding scenarios, i.e., mixing SO_2 with either liquid in the first module, were used for most of the runs in the subsequent experiments using both AFR-LF and AFR-G1.

IV. SO_2 absorption in water

Absorption in AFR-LF

Absorption runs with a constant gas flow rate (75mL min^{-1} at STP) at various SO_2 mole fractions were conducted at room temperature and three water flow rates in the AFR-LF. Table 3 details the experimental variables and calculated parameters from which the values of the overall mass transfer coefficients are obtained. Figure 2 shows the effects of SO_2 mole fraction and water flow rate on the SO_2 absorption rate and the liquid-side volumetric mass transfer coefficient, respectively.

Table 3 Details of overall mass transfer calculations for SO_2-water in AFR-LF (SO_2 mole fraction=0.933, T=22-25°C, A_1: water and A_2: SO_2-N_2)

QL(mL min^{-1})	$y_{A,in}$	$P_{t,in}$ (kPa)	C^*_{A1} (mol L^{-1})	$P_{t,out}$ (kPa)	C^*_{A2} (mol L^{-1})	C_{A2} (mol L-1)	$1/\tau$ (s^{-1})	ln(X)#	$K_La\times100$ (s^{-1})
0.3	0.636	231	2.02	148	1.21	1.1	0.00189	0.786	0.148±0.01
	0.737	231	2.33	148	1.42	1.32	0.00189	0.836	0.158±0.01
	0.824	258	2.91	148	1.6	1.73	0.00189	0.903	0.170±0.02
	0.933	231	2.96	145	1.82	1.86	0.00189	0.99	0.187±0.01
0.5	0.636	251	2.19	145	1.12	1.11	0.00314	0.707	0.22±0.01
	0.737	245	2.47	144	1.33	1.29	0.00314	0.736	0.231±0.01
	0.824	238	2.68	141	1.48	1.58	0.00314	0.891	0.280±0.01
	0.933	238	3.04	141	1.75	2	0.00314	1.07	0.337±0.01
0.7	0.636	258	2.24	144	1.06	1.04	0.0044	0.624	0.275±0.01
	0.737	258	2.6	141	1.24	1.27	0.0044	0.669	0.295±0.01
	0.824	231	2.61	137	1.4	1.46	0.0044	0.822	0.362±0.01
	0.933	231	2.95	134	1.63	1.88	0.0044	1.01	0.446±0.01

#Second term of Eq. (9)

Citation: Moniri A, Wang H, Wu X. Application of corrosion-resistant corning advanced-flow reactors for multiphase Bunsen reaction-part one: investigation on SO_2 absorption. *Int J Petrochem Sci Eng.* 2019;4(4):123–136. DOI: 10.15406/ipcse.2019.04.00112

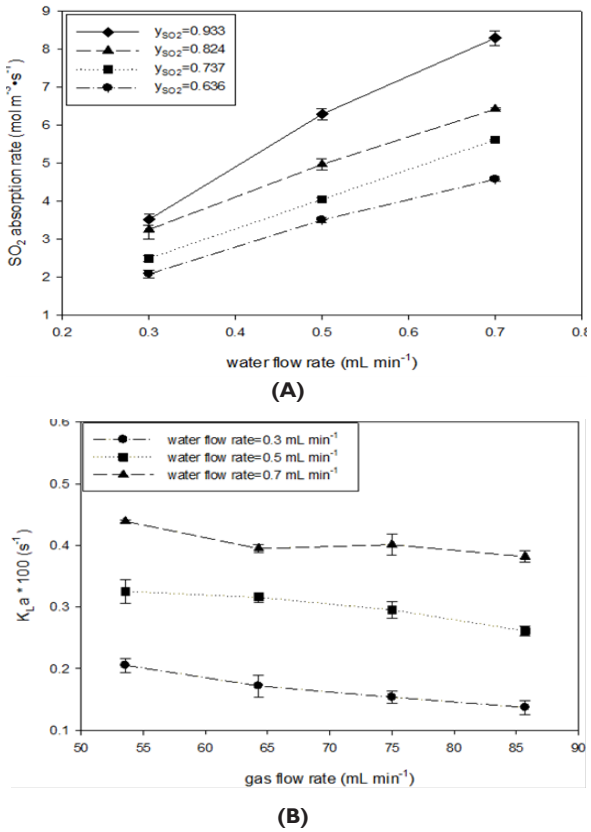

Figure 2 SO_2 absorption rate (A) and liquid-side volumetric mass transfer coefficient (B) vs. water flow rate in AFR-LF (Q_G = 75mL/min, T = 22-25°C, ports: A_1, water and A_2, SO_2-N_2).

At a constant mole fraction of sulfur dioxide, a sharp increase could be seen in sulfur dioxide absorption rate when the flow rate of water was increased. Increase in the mole fraction of SO_2 at a constant water flow rate also increased the SO_2 absorption rate. The higher the water flow rate, the stronger the increasing effect of the mole fraction of SO_2 on its absorption rate. The same trend was observed as well when plotting the volumetric mass transfer coefficients vs. water flow rate for four levels of SO_2 mole fraction. At lower water flow rate, the effect of mole fraction is insignificant because the resistance to mass transfer is on the liquid side where the K_La value is low. At higher water flow rate, the resistance is shifted to the gas side to some extent and the gradient of SO_2 in gas phase begins to play a role. Nieves-Remacha et al. studied the effects of operating conditions on the hydrodynamics of a water-CO_2 system using a AFR-G1.[16] They observed that the average bubble size and bubble size distribution depend on the gas and liquid flow rates. At the lower flow rate of water, most of the heart-shaped cells were occupied by large bubbles, which resulted in inadequate contact between the gas and liquid, and poor mass transfer across the interface. On the other hand, the bubble size decreased with increasing liquid flow (Q_L), which increased shear rates at the inlet of the heart-shaped cells. Greater turbulence in the water flow and increased specific area per volume of water resulted in larger K_La values.

Table 3 also shows that increasing the mole fraction of sulfur dioxide stabilized the equilibrium concentration of sulfur dioxide in the water at inlet C^*_{A1} and outlet C^*_{A2}, respectively, leading to an increase in volumetric mass transfer coefficients. Comparing the values of C^*_{A2} and C_{A2}, two different behaviors were observed. At low mole fraction values of sulfur dioxide, CA_2 stayed below the equilibrium values, while at high mole fractions, the latter was higher. This was mainly due to the higher partial pressure of sulfur dioxide at the inlet that made SO_2 dissolve quickly in water. However, when the pressure at the outlet dropped significantly, a new equilibrium was hard to reach and the outlet concentration C_{A2} became oversaturated.

Table 4 Details of overall mass transfer calculations for SO_2-water in LF-AFR (SO_2 mole fraction=0.933, T=22-25°C, A_1: water and A_2: SO_2-N_2)

QL (mL min^{-1})	QG (mL min^{-1})	$P_{t,in}$ (kPa)	C^*_{A1} (mol L^{-1})	$P_{t,out}$ (kPa)	C^*_{A2} (mol L^{-1})	C_{A2} (mol L^{-1})	1/τ (s^{-1})	ln(X)#	K_La×100 (s^{-1})
0.3	53.57	191	2.45	125	1.56	1.62	0.00189	1.09	0.205±0.01
	64.29	219	2.79	142	1.79	1.67	0.00189	0.91	0.172±0.02
	75	232	2.97	152	1.92	1.65	0.00189	0.814	0.154±0.02
	85.72	252	3.22	163	2.06	1.66	0.00189	0.725	0.137±0.01
0.5	53.57	205	2.62	125	1.53	1.69	0.00314	1.04	0.325±0.02
	64.29	219	2.8	131	1.63	1.77	0.00314	1	0.316±0.01
	75	239	3.06	142	1.76	1.86	0.00314	0.938	0.295±0.01
	85.72	259	3.31	152	1.9	1.87	0.00314	0.83	0.261±0.01
0.7	53.57	198	2.53	118	1.41	1.6	0.0044	0.998	0.439±0.01
	64.29	218	2.79	124	1.51	1.65	0.0044	0.897	0.395±0.01
	75	232	2.97	131	1.61	1.77	0.0044	0.911	0.401±0.02
	85.72	252	3.22	142	1.74	1.87	0.0044	0.867	0.382±0.01

#Second term of equation (9)

Absorption rates for a high mole fraction of gas (y_{SO2}=0.933) at various gas flow rates (at STP) were also measured at room temperature and three water flow rate levels. A high mole fraction was used to try to minimize the effect on the gas side. Table 4 shows the experimental variables and calculated parameters from which the values of mass transfer coefficients are obtained. Figure 3 depicts the effects of gas flow rate and water flow rate on the SO_2 absorption rate and the volumetric liquid-side mass transfer coefficient. At two lower water flow rates, no significant changes in SO_2 absorption rate were observed when the gas flow rate was increased, as shown in Figure 3 (A).

Citation: Moniri A, Wang H, Wu X. Application of corrosion-resistant corning advanced-flow reactors for multiphase Bunsen reaction-part one: investigation on SO_2 absorption. *Int J Petrochem Sci Eng.* 2019;4(4):123–136. DOI: 10.15406/ipcse.2019.04.00112

At the highest water flow rate, a small increase in absorption rate by gas flow was observed. The absorption capacity is determined by liquid flow once sufficient SO_2 is provided. However, the liquid-side volumetric mass transfer coefficients tended to decrease with increasing gas flow rate as shown in Figure 3 (B).

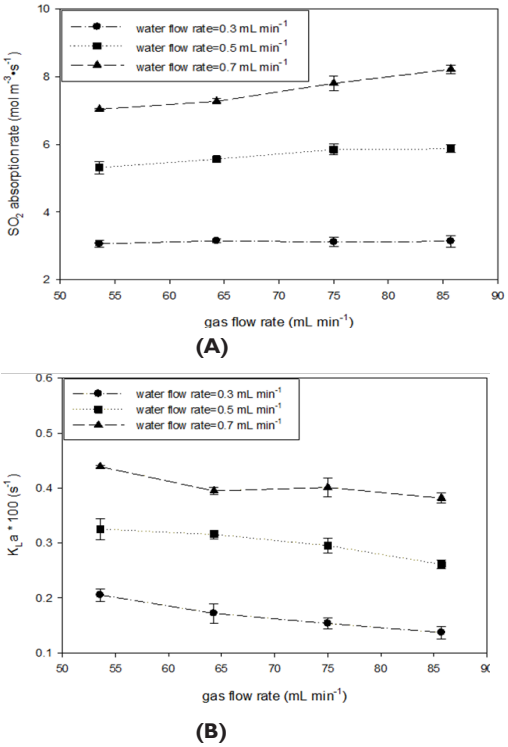

Figure 3 SO_2 absorption rate (A) and liquid-side volumetric mass transfer coefficient (B) vs. gas flow rate in AFR-LF (SO_2=0.933, T= 22-25°C, Ports:A1, water and A2, SO_2-N_2).

This confirms the argument that increasing the gas flow rate increases the average bubble size, which in turn reduces the specific interface area.[16] On the other hand, the absorption capacity was reached, resulting in quite similar outlet SO_2 concentrations in water C_{A2} for each level of water flow rate. Because of the resistance to flow, the increase in gas flow led to total pressure increase and thus the increase in C^*_{A1}. As a result, the logarithmic term of Eq. (9) began to decrease and then the coefficients became smaller. Comparing the values of C^*_{A2} to C_{A2}, oversaturation was also observed for most of the runs for SO_2 absorption in water. The third reason for a decrease in K_La with gas flow rate increase could be the effect on real residence time. At higher gas flow rate, the residence time determined by water flow rate was obviously longer than the real residence time. Then, the calculated K_La became smaller than it should be.

Absorption in AFR-G1

Absorption runs with a constant mole fraction of gas (y_{SO2}=0.50) at various gas flow rates at STP were conducted at room temperature and four water flow rate levels in the AFR-G1. provides the detailed experimental variables and calculated results. Figure 4 shows the effects of SO_2 flow rate and water flow rate on the SO_2 absorption rate and the volumetric liquid-side mass transfer coefficient, respectively. At a constant gas flow rate, a gradual increase in sulfur dioxide absorption could be seen when the water flow rate was increased. At a constant water flow rate, the absorption rate of sulfur dioxide was also increased steadily by increasing the gas flow rate. On the other hand, the volumetric mass transfer coefficient values were relatively stable with the change of the water flow rate at 1600 mL min^{-1} of the gas flow rate. While the data of K_La vs. water flow at 1800 and 2000 mL min^{-1} gas flow rates overlapped at larger values, they tended to decline marginally with the increase in water flow rates. This observation differs from the findings in the AFR-LF as well as the result from the study of the CO_2-water system by Nieves-Remacha et al.[16] As can be seen from Table 5, at a constant gas flow rate, the value of C_{A2} was reduced by increasing the flow rates of water, while C^*_{A1} was increased, the larger gap between the two concentrations resulted in smaller values of the second term of Eq. (9). On the other hand, the residence time was reduced, which in turn resulted in an increase of 1/τ values.

Table 5 Details of overall mass transfer calculations for SO_2-water in G1-AFR (SO_2 mole fraction=0.50, T=22-25°C, A_1: water and A_2: SO_2-N_2).

QL (mL min^{-1})	QG (mL min^{-1})	$P_{t,in}$ (kPa)	C^*_{A1} (mol L^{-1})	$P_{t,out}$ (kPa)	C^*_{A2} (mol L^{-1})	C_{A2} (mol L^{-1})	1/τ (s^{-1})	ln(X)#	K_La×100(s^{-1})
	1600	191	1.31	102	0.45	0.63	0.0625	0.657	4.10±0.02
30	1800	184	1.26	102	0.47	0.66	0.0625	0.745	4.66±0.04
	2000	205	1.4	102	0.46	0.75	0.0625	0.761	4.75±0.03
	1600	205	1.4	102	0.38	0.49	0.0937	0.43	4.03±0.02
45	1800	205	1.4	102	0.4	0.54	0.0937	0.482	4.51±0.01
	2000	226	1.55	102	0.4	0.6	0.0937	0.487	4.56±0.02
	1600	219	1.5	102	0.35	0.48	0.104	0.383	3.98±0.02
50	1800	226	1.55	102	0.36	0.52	0.104	0.411	4.27±0.01
	2000	240	1.64	102	0.38	0.56	0.104	0.416	4.33±0.01
	1600	226	1.55	102	0.33	0.41	0.125	0.307	3.83±0.01
60	1800	240	1.64	102	0.33	0.46	0.125	0.329	4.11±0.02
	2000	260	1.78	102	0.34	0.5	0.125	0.332	4.14±0.02

#Second term of equation (9)

Citation: Moniri A, Wang H, Wu X. Application of corrosion-resistant corning advanced-flow reactors for multiphase Bunsen reaction-part one: investigation on SO_2 absorption. *Int J Petrochem Sci Eng.* 2019;4(4):123–136. DOI: 10.15406/ipcse.2019.04.00112

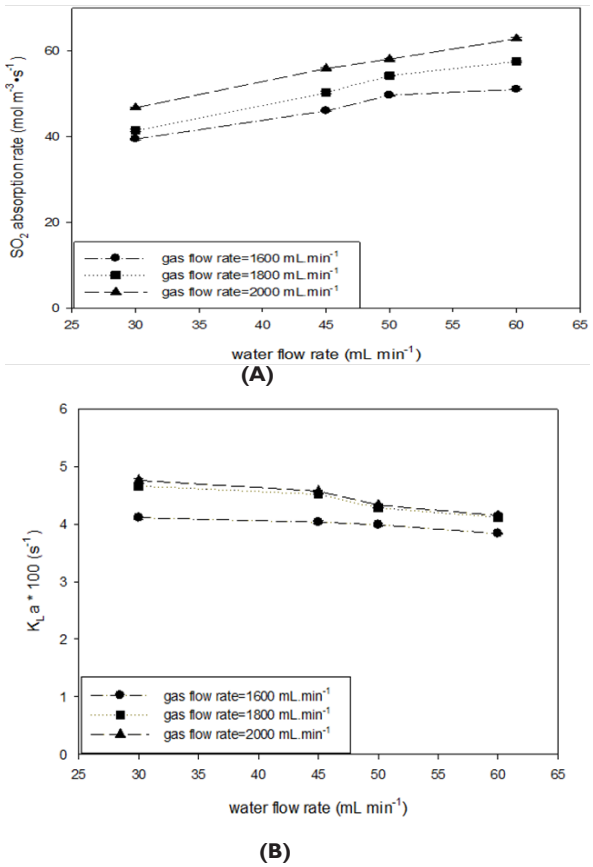

Figure 4 SO_2 absorption rate. (A) Liquid-side volumetric mass transfer coefficient. (B) vs. water flow rate in AFR-G1 (y_{SO2} = 0.50, T = 22-25°C, ports: A_1, water and A_2, SO_2-N_2).

At these critical conditions, the effect of shortening the residence time and the change of SO_2 concentrations by gas and water flow rates balanced, leading to relatively stable volumetric mass transfer coefficients. While the shortening of residence time by increasing the water flow tipped the scales, a decrease of the coefficients was observed. At constant values of water flow, the increase of gas flow from 1600 to 1800 mL min^{-1} led to a relatively small increase in K_La; however further increase in gas flow rate resulted in no further change in K_La. This may indicate that the mass transfer in absorption was not controlled by the SO_2 transportation on the gas side.

V. SO_2 absorption in toluene

Absorption in AFR-LF

In runs similar to those using water as solvent for SO_2 absorption, the solvent as switched toluene and the absorption was first run with a given gas flow rate (75 mL/min at STP) at four levels of SO_2 mole fraction (0.636–0.933), three toluene flow rate levels (0.65–12.7 mL min^{-1}), and at room temperature. Table 6 details the experimental variables and the calculated results.

Compared to Table 3, the flow rate range of toluene was two times that of water. This is roughly determined by the stoichiometry of the Bunsen reaction, the solubility of iodine in toluene and water, and the excessive use of water. (When multiphase absorption and the Bunsen reaction (part two) are carried out with iodine-toluene solution, the flow rate of toluene used can be 2 to 4 times that of water.) This also means that, relative to the same levels of SO_2 flow rate, higher flow rate of toluene was used than that of water. Table 6 also shows that thevalues of the outlet equilibrium concentrations C^*_{A2} are always larger than the outlet concentration C_{A2} of SO_2 in toluene, indicating that absorption equilibrium has not been achieved in toluene absorption. Unlike in water absorption, no oversaturated absorption was observed for toluene. Figure 5 depicts the effects of SO_2 mole fraction and toluene flow rate on the SO_2 absorption rate and the volumetric liquid-side mass transfer coefficient.

The absorption rate was reduced by increasing SO_2 mole fractions and toluene flow rates, which can be explained by the increase in absorption driving force. The higher values of K_La at higher mole fraction of SO_2 may imply resistance to mass transfer on the gas side, and the increasing K_La values at higher toluene flow rate means greater interface areas between gas and liquid for a unit volume of liquid.

Table 6 Details of overall mass transfer calculations for SO_2-toluene in LF-AFR (gas flow rate=75mL min^{-1}, T=22-25°C, A_1: toluene and A_2: SO_2-N_2).

QL(mL min^{-1})	$y_{A,in}$	$P_{t,in}$ (kPa)	C^*_{A1} (mol L^{-1})	$P_{t,out}$ (kPa)	C^*_{A2} (mol L^{-1})	C_{A2} (mol L-1)	$1/\tau$ (s^{-1})	ln(X)#	$K_La\times100$ (s^{-1})
0.65	0.636	202	5.78	133	2.67	1.8	0.004	0.373	0.149±0.01
	0.737	202	6.69	126	3.08	2.22	0.004	0.404	0.162±0.01
	0.824	202	7.48	123	3.59	2.59	0.004	0.425	0.170±0.01
	0.933	169	7.08	116	4.22	3.41	0.004	0.658	0.263±0.01
0.9	0.636	217	6.2	130	2.31	1.47	0.00563	0.271	0.152±0.01
	0.737	210	6.96	124	2.65	1.84	0.00563	0.307	0.173±0.01
	0.824	204	7.52	120	3.14	2.16	0.00563	0.339	0.191±0.01
	0.933	176	7.36	109	3.56	2.83	0.00563	0.484	0.273±0.01
1.27	0.636	238	6.78	127	1.83	1.22	0.00797	0.199	0.158±0.01
	0.737	231	7.62	120	1.93	1.56	0.00797	0.228	0.182±0.01
	0.824	203	7.52	116	2.55	1.73	0.00797	0.261	0.208±0.01
	0.933	177	7.41	107	2.86	2.2	0.00797	0.353	0.281±0.01

#Second term of equation (9)

Citation: Moniri A, Wang H, Wu X. Application of corrosion-resistant corning advanced-flow reactors for multiphase Bunsen reaction-part one: investigation on SO_2 absorption. *Int J Petrochem Sci Eng.* 2019;4(4):123–136. DOI: 10.15406/ipcse.2019.04.00112

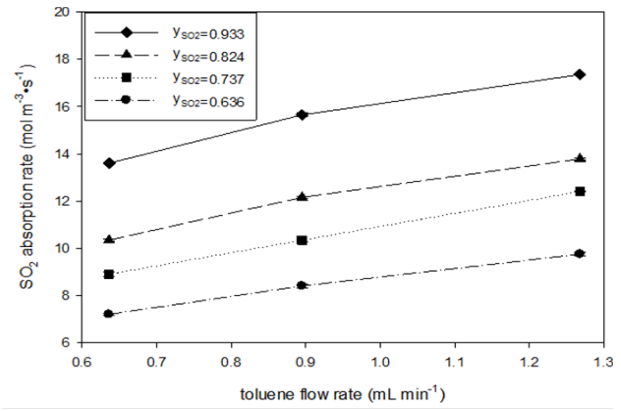

(A)

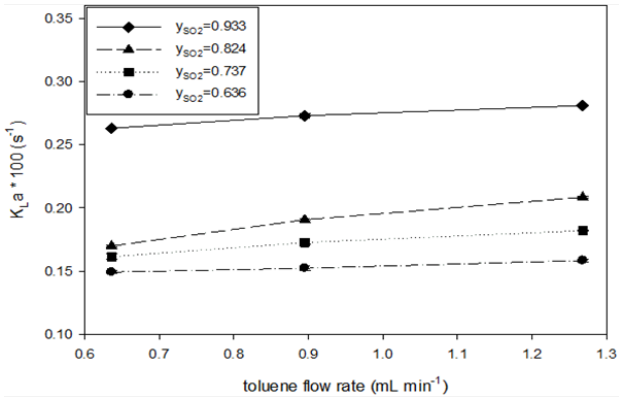

(B)

Figure 5 SO_2 absorption rate. (A) Liquid-side volumetric mass transfer coefficient. (B) vs. toluene flow rate in AFR-LF (Q_G = 75mL/min, T = 22-25°C, ports: A_1, toluene and A_2, SO_2-N_2)

Comparing the effects of water and toluene flow rate on SO_2 absorption, it was found that the increase of absorption rate and the volumetric mass transfer coefficient with water flow rate is sharper than that with toluene flow rate. At a similar liquid flow rate (water at 0.7 mL min^{-1} and toluene at 0.65 mL min^{-1}) with the range of SO_2 mole fraction in gas phase (0.646–0.933), toluene showed higher absorption rates (7–13.5 mol m^{-3}s^{-1}) than water (4.2–8.4 mol m^{-3}s^{-1}); however, water had higher values of the volumetric mass transfer coefficient (0.0028–0.0047 s^{-1}) than toluene (0.0015–0.0026 s^{-1}). The higher absorption rate in toluene can also be attributed to differences in the driving force of mass transfer. The solubility of SO_2 in toluene is more than 10 times its solubility in water. With the same partial pressure of SO_2 in gas, the mass transfer driving force, $C_A^* - C_A$, would be 10 times that in toluene initially when C_A is zero. The lower $K_L a$ for toluene may be because the specific interface area in toluene is smaller than in water and the diffusivity of SO_2 is smaller in toluene than in water.

Absorption rates at various gas flow rates (at STP) with a high mole fraction of SO_2 (SO_2 =0.933) were also measured at room temperature and three toluene flow rate levels. High SO_2 mole fraction was used to minimize gas-side mass transfer resistance. Table 7 gives the detailed experimental variables and calculated results. Figure 6 shows the effects of gas flow rate on the SO_2 absorption rate and the volumetric liquid-side mass transfer coefficient. At a constant toluene flow rate, SO_2 absorption rate and mass transfer coefficients were sharply increased with gas flow rates. This behavior is different from what has been observed in SO_2-water systems where the absorption rate seemed to be independent of the gas flow rate and the $K_L a$ value decreased with increasing gas flow. However, this observation is in agreement with Nieves-Remacha et al.,[16] where increase in flow rate of each gas and liquid phase has a positive effect on the volumetric mass transfer coefficient of CO_2 into water. It is believed that the increase in $K_L a$ with increasing gas flow is due to the increase in specific interfacial area.

Table 7 Details of overall mass transfer calculations for SO_2-toluene in LF-AFR (SO_2 mole fraction=0.933, T=22-25°C, A_1: toluene and A_2: SO_2-N_2).

QL (mLmin^{-1})	QG (mL min^{-1})	$P_{t,in}$ (kPa)	C^*_{A1} (mol L^{-1})	$P_{t,out}$ (kPa)	C^*_{A2} (mol L^{-1})	C_{A2} (mol L^{-1})	1/τ (s^{-1})	ln(X)#	$K_L a$×100(s^{-1})
0.65	53.57	148	6.21	95	3.14	2.81	0.004	0.603	0.241±0.01
	64.29	162	6.79	109	3.82	3.14	0.004	0.622	0.249±0.01
	75	169	7.08	116	4.22	3.41	0.004	0.658	0.263±0.01
	85.72	176	7.31	119	4.41	3.76	0.004	0.723	0.289±0.01
0.9	53.57	148	6.21	95	2.65	2.2	0.00563	0.438	0.247±0.01
	64.29	162	6.79	95	2.9	2.54	0.00563	0.469	0.264±0.01
	75	176	7.36	109	3.56	2.83	0.00563	0.484	0.273±0.01
	85.72	183	7.65	112	3.81	3.11	0.00563	0.522	0.294±0.01
1.27	53.57	142	5.96	96	2.02	1.65	0.00797	0.324	0.258±0.01
	64.29	158	6.63	96	2.33	1.94	0.00797	0.346	0.276±0.01
	75	177	7.41	107	2.86	2.2	0.00797	0.353	0.281±0.01
	85.72	184	7.69	110	3.16	2.46	0.00797	0.385	0.307±0.01

Second term of equation (9)

Citation: Moniri A, Wang H, Wu X. Application of corrosion-resistant corning advanced-flow reactors for multiphase Bunsen reaction-part one: investigation on SO_2 absorption. *Int J Petrochem Sci Eng.* 2019;4(4):123–136. DOI: 10.15406/ipcse.2019.04.00112

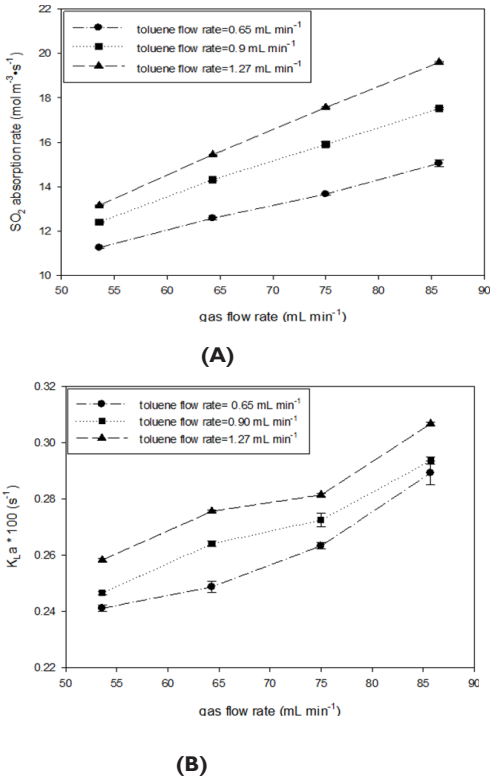

Figure 6 SO_2 absorption rate (A) and liquid-side volumetric mass transfer coefficient (B) vs. gas flow rate in AFR-LF (y_{SO2} = 0.933, T = 22-25°C, ports:A_1, toluene and A_2, SO_2-N_2).

Absorption in AFR-G1

Absorption runs with a constant gas mole fraction (SO_2=0.50) at various SO_2 flow rates at STP were conducted at room temperature and four toluene flow rate levels. Table 8 shows the exp eriment variables and calculated results. Figure 7 shows the effects of increasing gas and toluene flow rates on the SO_2 absorption rate and the liquid-side volumetric mass transfer coefficient. Increasing the toluene flow rate led to an increase in the absorption rate values in the beginning (Figure 7 (A)); however, the data became constant at the higher flow rate of toluene. At each level of toluene flow rate, the effect of increasing gas flow on the absorption rate appeared more obvious, similar to what was observed using the AFR-LF. In Figure 7 (B), the K_La values seem to be insensitive to both toluene and gas flow rates, which is similar to the observation for the AFR-LF. Increasing the toluene flow rate by a factor of two maintained the K_La values at the same margin (0.011–0.014s^{-1}). At lower toluene flow, the K_La value change by gas flow increasing from 1600 to 2000 mL min^{-1} (40% increase) is negligible (<3 %) Even at higher toluene flow, this change is still small (<15 %). However, the K_La value obtained in the AFR-G1 is 4-6 times that obtained in the AFR-LF.

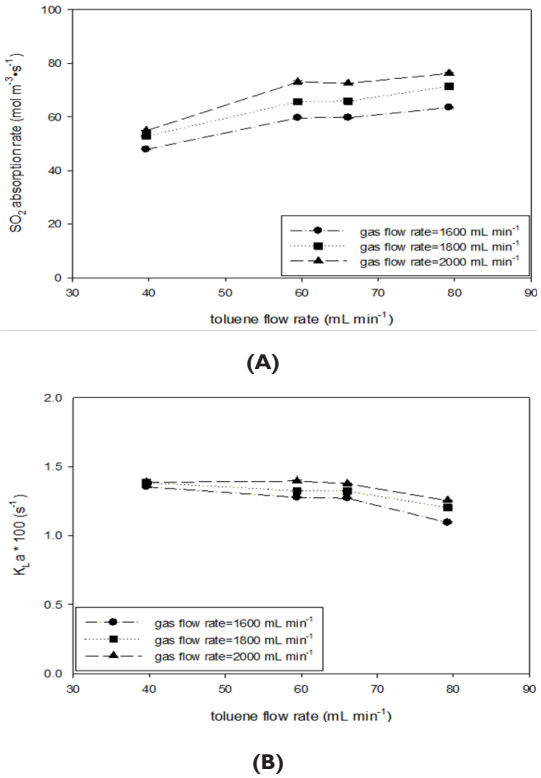

Figure 7 SO_2 absorption rate (A) and liquid-side volumetric mass transfer coefficient (B) vs. toluene flow rate in AFR-G1 (y_{SO2} = 0.50,T = 22-25°C, ports: A_1, toluene and A_2, SO_2-N_2).

Table 8 Details of overall mass transfer calculations for SO_2-toluene in AFR-G1. (SO_2 mole fraction=0.50, T=22-25°C, A_1: toluene and A_2: SO_2-N_2).

QL (mLmin^{-1})	QG (mLmin^{-1})	$P_{t,in}$ (kPa)	C^*_{A1} (mol L^{-1})	$P_{t,out}$ (kPa)	C^*_{A2} (mol L^{-1})	C_{A2} (mol L^{-1})	1/τ (s^{-1})	ln(X)#	K_La×100(s^{-1})
39.63	1600	171	3.83	102	0.37	0.58	0.0826	0.164	1.35±0.01
	1800	185	4.14	102	0.38	0.64	0.0826	0.168	1.38±0.01
	2000	192	4.3	102	0.41	0.66	0.0826	0.168	1.39±0.01
59.45	1600	219	4.92	102	0.23	0.48	0.124	0.103	1.28± 0.01
	1800	233	5.23	102	0.25	0.53	0.124	0.107	1.33±0.01
	2000	247	5.54	102	0.25	0.59	0.124	0.113	1.40±0.01
66.06	1600	219	4.92	102	0.23	0.43	0.138	0.092	1.27± 0.01
	1800	233	5.23	102	0.24	0.48	0.138	0.096	1.32±0.01
	2000	247	5.54	102	0.25	0.53	0.138	0.1	1.38±0.01
79.26	1600	267	6	102	0.18	0.38	0.165	0.066	1.10±0.01
	1800	274	6.15	102	0.18	0.43	0.165	0.073	1.20±0.01
	2000	281	6.31	102	0.21	0.46	0.165	0.076	1.26±0.01

Second term of equation (9)

Citation: Moniri A, Wang H, Wu X. Application of corrosion-resistant corning advanced-flow reactors for multiphase Bunsen reaction-part one: investigation on SO_2 absorption. *Int J Petrochem Sci Eng.* 2019;4(4):123–136. DOI: 10.15406/ipcse.2019.04.00112

VI. SO_2 absorption in water-toluene mixture

Absorption in AFR-LF

Absorption runs with a constant mole fraction of SO_2 (y_{SO2}=0.933) and liquid flow rate (1.5 mL min^{-1}) at various gas flow rates at STP were conducted at room temperature (22–25°C) for SO_2 in water-toluene mixture where the gas phase resistance was negligible. The purpose of this experiment was to understand the effects of increasing water volumetric fraction in water-toluene and SO_2 flow rate in SO_2-N_2 mixtures in the described system as shown in Figure 8 (A). By definition water volumetric fraction equals water flow rate divided by total liquid flow rate. As can be seen, at a constant water fraction, a sharp increase could be seen in sulfur dioxide absorption rate when the flow rate of SO_2 was increased from 53.57 to 85.72 mL min^{-1}. The lower the water fraction, the stronger the increasing effect of the SO_2 flow rate on its absorption rate. On the other hand, an increase in water fraction at a constant gas flow rate decreased the SO_2 absorption rate. This decreasing trend was less tangible at lower water fraction rate when mixture was mainly consisted of toluene. The absorption runs were repeated at room temperature with constant mole fraction of gas (y_{SO2}=0.933) and constant water volumetric fraction at various gas flow rates at STP and five liquid flow rate levels as shown in Figure 8 (B).

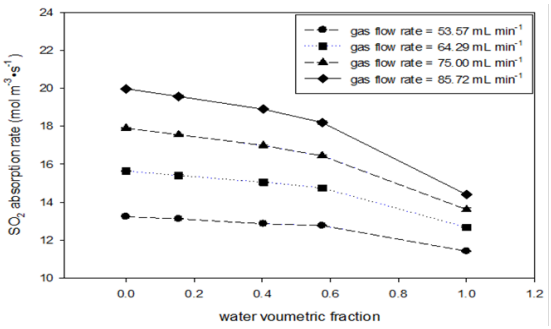

(A)

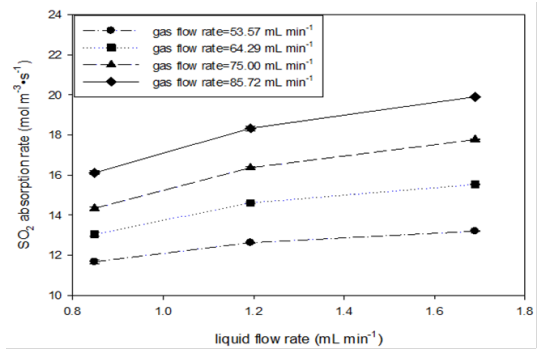

(B)

Figure 8 (A) SO_2 absorption rate vs. water volumetric fraction in AFR-LF and (B) SO_2 absorption rate versus liquid flow rate in the AFR-LF (liquid flow rate=1.5 mL/min for Fig.8 (A), water volumetric fraction=0.25 for Fig.8 (B), mole fraction of SO_2=0.933, T=22-25°C, ports A_1, toluene, A_2, SO_2-N_2 and A_3, Water).

Clearly, at all gas levels, enhancing liquid flow rates increased the absorption rates. However, larger liquid flow rates gave a smoother rise to absorption values mainly due to the fact that complete absorption of SO_2 in toluene was more likely achieved at larger liquid flow rates. Similar to Figure 8 (B), absorption rates of SO_2 were increased at a constant liquid flow rate by increasing gas flow rates, leading to an increase in mass transfer at high flow rates. The observation in this section confirms the argument in previous sections where the higher absorption rate in toluene was attributed to differences in the driving force of mass transfer due to higher solubility of SO_2 in toluene than in water. In the following section, similar experiments were conducted for the ternary SO_2-water-toluene system in AFR-G1 at a constant water volumetric fraction.

Absorption in AFR-G1

The absorption runs with a constant mole fraction of gas (y_{SO2}=0.50) and water volumetric fraction (0.15) at various gas flow rates at STP were conducted at room temperature (22–25°C) and four liquid flow rate levels. Figure 9 shows the effects of the liquid flow rate and gas flow rate on the SO_2 absorption rate. Increasing the liquid flow rates smoothly increased the absorption rates. An increase in gas flow rates also increased the absorption rates of SO_2 at a constant liquid flow rate which is fairly similar to what was observed in AFR-LF.

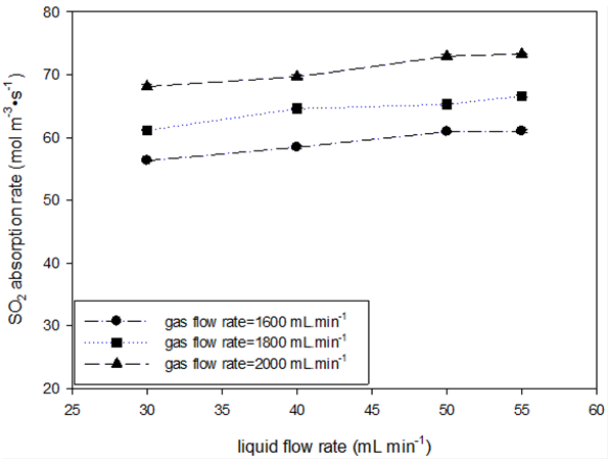

Figure 9 SO_2 absorption rate versus liquid flow rate in the AFR-G1 (mole fraction of SO_2=0.50, water volumetric fraction =0.15, T=22-25°C, ports A_1, SO_2-N_2, A_2, toluene and A_3, Water).

Scalability study of SO_2 absorption in LF and G1

The foregoing discussion is not definitive concerning the scalability of the two levels of AFR's. Specifically, the results showing the effect of water flow rate on K_La from the AFR-LF is not in agreement with that from the AFR-G1. The K_La values of the SO_2-water and SO_2-toluene absorption for both AFRs are not in the same order of magnitude either. Experiments using different numbers of modules of AFR-LF (one vs. five) for two systems (SO_2-water and SO_2-toluene) resulted in the same magnitude of overall absorption rate and a different order of magnitude for K_La Table 9 and Table 10.

Table 9 Comparison of SO_2-water absorption runs in AFR-LF using different fluidic modules

	One-fluidic module AFR-LF		Five-fluidic module AFR-LF	
QL (mL min^{-1})	SO_2 absorption×10^6 (mol s^{-1})	K_La×100 (s^{-1})	SO_2 absorption×10^6 (mol s^{-1})	K_La×100 (s^{-1})
0.3	7.55	1.18	8.11	0.205
0.5	13.1	1.9	14.1	0.325
0.7	18.5	2.55	18.7	0.439
1	24.5	3.19	25.1	0.545

Citation: Moniri A, Wang H, Wu X. Application of corrosion-resistant corning advanced-flow reactors for multiphase Bunsen reaction-part one: investigation on SO_2 absorption. *Int J Petrochem Sci Eng.* 2019;4(4):123–136. DOI: 10.15406/ipcse.2019.04.00112

Table 10 Comparison of SO_2-toluene absorption runs in AFR-LF using different fluidic modules.

	One-fluidic module AFR-LF		Five-fluidic module AFR-LF	
Q_L (mL min^{-1})	SO_2 absorption×10^6 (mol s^{-1})	K_La×100 (s^{-1})	SO_2 absorption×10^6 (mol s^{-1})	K_La×100 (s^{-1})
0.65	29.7	1.66	29.8	0.241
0.9	32.6	1.69	32.9	0.247
1.27	34.8	1.7	34.9	0.258
1.5	35	1.71	35.1	0.266

The values of K_La from one module are about 6–7 times those from five modules. This indicates that the absorption has been completed in one module and that the remaining modules contribute negligibly to the absorption, which merely extends the residence time and results in smaller K_La from the AFR-LF as in previous sections. Therefore, absorption runs were conducted using one single-module AFR-LF, as described in this section. Then, the new SO_2 absorption results of the one single module AFR-LF are compared with the results of the SO_2 absorption runs using the AFR-G1, where a single module was used. K.F. Jensen's group at MIT studied the scalability of these two scales of AFRs for liquid-liquid mass transfer.[23] The method that was used was to plot the K_La values vs. the residence time for both AFRs. By analyzing the magnitude of the K_La and the curves of K_La vs. residence time, the scalability across these two sizes of the AFR is evaluated. Figure 10 plots the K_La of SO_2 absorption in water and toluene using one-module LF and G1 vs. residence time.

Due to the significant differences in channel sizes and heart-shape cell layout, the smooth change of the K_La vs. residence time across the two levels of ARFs and the relatively similar magnitudes of volumetric mass transfer coefficients indicate seamless scalability of the AFR. The shape of K_La vs. residence time for SO_2-water is the same as that for the liquid-liquid system in;[23] however, the shape for the SO_2-toluene system is different. The changes in polarity, viscosity, and surface tension of the solvent may change the mass transfer behavior for a given gas in the same AFR.

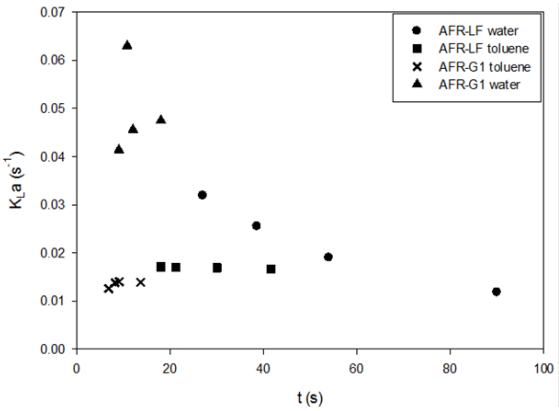

Figure 10 Liquid-side volumetric mass transfer coefficients vs. liquid residence time (t) in AFRs for SO_2 absorption in water and toluene at room temperature.

Conclusion

To study low-temperature Bunsen reaction using iodine-toluene solution in the H_2S splitting cycle for hydrogen production, the absorption behavior of SO_2 in water and toluene was studied in the absence of iodine and the scalability of mass transfer across both micro-and milli-scales of the AFR modules was evaluated. The following conclusions can be drawn from this study:

i. For both SO_2-water and SO_2-toluene absorption systems, varying the mole fraction of SO_2 in gas phase indicates that the gas-side mass transfer resistance is significant.

ii. For an SO_2-water system using the AFR-LF, increasing the liquid flow rate at a fixed gas flow rate results in an increase in SO_2 absorption rate and the liquid-side volumetric mass transfer coefficient. However, increasing the gas flow rate at a fixed liquid flow rate results in only insignificant change in SO_2 absorption rate and a slight drop in the liquid-side volumetric mass transfer coefficient. Using the AFR-G1, increasing both gas and liquid flow shows insignificant effect on both absorption rate and liquid-side volumetric mass transfer coefficient.

iii. For SO_2-toluene system using the AFR-LF at a fixed liquid flow rate, increasing gas flow rate results in an increase in SO_2 absorption rate and the liquid-side volumetric mass transfer coefficient. However, at a fixed gas flow rate, the increase in liquid flow rate just leads to an increase in absorption rate and insignificant change in the liquid-side volumetric mass transfer coefficient. Using the AFR-G1, the increase in the gas and liquid flow rates leads to an increase in absorption rate and insignificant change in the liquid-side volumetric mass transfer coefficient. Even at lower gas flow rates, increasing liquid flow rate leads to a decrease in the mass transfer coefficient.

iv. For SO_2-water-toluene system, SO_2 had higher solubility in toluene than water due to differences in the driving force for mass transfer in both AFR-LF and AFR-G1.

v. The magnitude of the liquid-side volumetric mass transfer coefficient and its change with residence time indicate straightforward and seamless scalability across both the LF- and G1 scales of the AFR.

Nomenclature

a	Interfacial area per unit volume of the reactor, $m^2m^{-3;}$
C_A	Concentration at any point in the reactor, mol m^{-3}
C_A^*	Equilibrium concentration of A at the interface of gas and liquid, mol m^{-3}
C_t	Total concentration in the liquid phase, mol m^{-3}
C_{Ai}^*	Equilibrium concentration of A (i=1 inlet, i=2 outlet of the reactor), mol m^{-3}
D_A	Diffusivity of A in the gas phase, m^2s^{-1}
F_G	Molar flow rate of inert in the gas phase, mol s^{-1}
F_L	Molar flow rate of inert gas in the liquid phase, mol s^{-1}
H_A	Henry's coefficient, Pa m^3mol^{-1}
k_G	Gas-side mass transfer coefficient, mol $m^{-2}Pa^{-1}s^{-1}$

Citation: Moniri A, Wang H, Wu X. Application of corrosion-resistant corning advanced-flow reactors for multiphase Bunsen reaction-part one: investigation on SO_2 absorption. *Int J Petrochem Sci Eng.* 2019;4(4):123–136. DOI: 10.15406/ipcse.2019.04.00112

k_L	Liquid-side mass transfer coefficient, m s^{-1}
K_Ga	Gas-side volumetric mass transfer coefficient, mol $m^{-3}Pa^{-1}s^{-1}$
K_La	Liquid-side volumetric mass transfer coefficient, s^{-1}
K_{eq}	Equilibrium constant
N_A	Flux of straight mass transfer at any point in the reactor, mol $m^{-2}s^{-1}$
n	Number of moles, kmol
P_A	Partial pressure of A in the bulk of gas, Pa
P_A'	Partial pressure of A at the interface of gas and liquid, Pa
P_t	Total pressure in the gas phase, Pa
Q_G	Volumetric gas flow rate, mL min^{-1}
Q_L	Volumetric liquid flow rate, mL min^{-1}
T	Temperature, K (or °C)
Vr	Reactor volume, mL (or m^3)
y_{SO2}	mole fraction of SO_2 in gas phase
z	Film thickness, m
Z	Coordinates, m

Greek letters

τ	Residence time, s
μ	Viscosity, Pa s
ρ	Density, kg m^{-3}

Abbreviations

GA	General Atomics
AFR-G1	G1 Standard Evaluation Advanced-Flow Reactor
AFR-LF	Low Flow Advanced-Flow Reactor
S-I	Sulfur-Iodine
SRM	Steam Reforming of Methane
TCD	Thermal Conductivity Detector
UV-Vis	Ultraviolet-Visible Spectrophotometer

Acknowledgments

The authors gratefully acknowledge the Strategic Grant provided by the Natural Science and Engineering Research Council of Canada (NSERC STPGP-350428-07) as well as the Mitacs Globalink Research award. Many thanks to Corning Reactor Technology Center (China) for allowing us to use their AFR-G1 setup and to Changzhou University for their SO_2 analysis support.

Conflicts of interest

The author declares that there are no conflicts of interest.

References

1. Laureshen CJ. From oil sand bitumen to petrochemical feedstock. *Oil and Gas Processing Review*. 2006.
2. Wang H. Hydrogen production from a chemical cycle of H_2S splitting. *Inter J of Hydrogen Energy*. 2007;32(16):3907–3914.
3. Brown LC, Besenbruch G, Lentsch R, et al. *Alternative flowsheets for the sulfur–iodine thermochemical hydrogen cycle: United States*. Department of Energy. Oakland Operations Office. 2003.
4. Funk JE. Thermochemical hydrogen production: past and present. *Inter J of Hydrogen Energy*. 2001;26(3):185–190.
5. Giaconia A, Caputo G, Ceroli A, et al. Experimental study of two phase separation in the Bunsen section of the sulfur–iodine thermochemical cycle. *Inter J of Hydrogen Energy*. 2007;32(5):531–536.
6. Norman JH, Besenbruch GE, O'Keefe DR. *Thermochemical Water–Splitting for Hydrogen Production, GRI–80/0105*. Gas Research Institute. 1981.
7. Sakurai M, Nakajima H, Onuki K, et al. Investigation of 2 liquid phase separation characteristics on the iodine–sulfur thermochemical hydrogen production process. *Inter J of Hydrogen Energy*. 2000;25(7):605–611.
8. Sakurai M, Nakajima H, Amir R, et al. Experimental study on side–reaction occurrence condition in the iodine–sulfur thermochemical hydrogen production process. *International Journal of Hydrogen Energy*. 2000;25(7):613–619.
9. De Beni G, Pierini G, Spelta B. The reaction of sulphur dioxide with water and a halogen. The case of iodine: reaction in presence of organic solvents. *International Journal of Hydrogen Energy*. 1980;5(2):141–149.
10. Nomura M, Fujiwara S, Ikenoya K, et al. Application of an electrochemical membrane reactor to the thermochemical water splitting IS process for hydrogen production. *Journal of Membrane Science*. 2004;240(1–2):221–226.
11. Nomura M, Nakao S-i, Okuda H, et al. Development of an electrochemical cell for efficient hydrogen production through the IS process. *AIChE Journal*. 2004;50(8):1991–1998.
12. Sau S, Giaconia A, Caputo G, et al. Decrease the rate of recycling agents in the sulfur–iodine cycle by solid phase separation. *International Journal of Hydrogen Energy*. 2008;33(22):6439–6444.
13. Wang H, Le Person A, Zhao X, et al. A low-temperature hydrogen production process based on H_2S splitting cycle for sustainable oil sands bitumen upgrading. *Fuel Processing Technology*. 2013;108:55–62.
14. Fan Y, Herz RK. Measurement and enhancement of gas-liquid mass transfer in milliliter-scale slurry reactors. *Chemical Engineering Science*. 2007;62(21):5940–5951.
15. Li J, Moniri A, Wang H. Apparent kinetics of a gas–liquid–liquid system of Bunsen reaction with iodine-toluene solution for hydrogen production through H2S splitting cycle. *International Journal of Hydrogen Energy*. 2015;40(7):2912–2920.
16. Nieves Remacha MJ, Kulkarni AA, Jensen KF. Gas-Liquid Flow and Mass Transfer in an Advanced Flow Reactor. *Industrial & Engineering Chemistry Research*. 2013;52(26):8996–9010.
17. Lavric ED, Woehl P. Advanced–Flow™ glass reactors for seamless scaleup. *Chemistry Today*. 2009;27:45–48.
18. Chivilikhinl MS, Kuandykovl L, Lavric ED, et al. Residence Time Distribution in Corning® Advanced-Flow™ Reactors. Experiment and Modelling. *Chemical Engineering Transactions*. 2011;25:791–796.

19. Lavric ED. *Thermal performance of Corning glass microstructures*. Proceedings of the Heat Transfer and Fluid Flow in Microscale III Conference. 2008.

20. Braune S, Pöchlauer P, Reintjens R, et al. Selective nitration in a microreactor for pharmaceutical production under CGMP conditions. *Chemistry Today*. 2009;27:26–29.

21. Grob RL, Barry EF. *Modern practice of gas chromatography, 4th ed*. 2004.

22. Levenspiel O. Chemical reaction engineering. Industrial & Engineering Chemistry Research. 1999;38:4140–3.

23. Woitalka A, Kuhn S, Jensen KF. Scalability of mass transfer in liquid–liquid flow. *Chemical Engineering Science*. 2014;116:1–8.

24. Chivilikhinl MS, Kuandykovl L, Lavric ED, et al. Residence Time Distribution in Corning® Advanced–Flow™ Reactors. Experiment and Modelling. *Chemical Engineering Transactions*. 2011;25:791–796.

Citation: Moniri A, Wang H, Wu X. Application of corrosion-resistant corning advanced-flow reactors for multiphase Bunsen reaction-part one: investigation on SO_2 absorption. *Int J Petrochem Sci Eng.* 2019;4(4):123–136. DOI: 10.15406/ipcse.2019.04.00112